Secretory vesicle trafficking in awake and anaesthetized mice

Knabbe, Johannes; Nassal, Joris Paul; Verhage, Matthijs; Kuner, Thomas

published in
Journal of Physiology
2018

DOI (link to publisher)
10.1113/JP276022

document version
Publisher's PDF, also known as Version of record

J Physiol 596.16 (2018) pp 3759–3773

The Journal of Physiology

Secretory vesicle trafficking in awake and anaesthetized mice: differential speeds in axons *versus* synapses

Johannes Knabbe[1], Joris Paul Nassal[1,2], Matthijs Verhage[2] and Thomas Kuner[1]

[1] *Department of Functional Neuroanatomy, Institute for Anatomy and Cell Biology, Heidelberg University, Im Neuenheimer Feld 307, 69120, Heidelberg, Germany*

[2] *Departments of Functional Genomics and Clinical Genetics, Center for Neurogenomics and Cognitive Research (CNCR), VU University Amsterdam and VU University Medical Center, De Boelelaan, 1087, 1081 HV Amsterdam, The Netherlands*

Edited by: Jaideep Bains & Katalin Toth

Key points

- Despite their immense physiological and pathophysiological importance, we know very little about the biology of dense core vesicle (DCV) trafficking in the intact mammalian brain.
- DCVs are transported at similar average speeds in the anaesthetized and awake mouse brain compared to neurons in culture, yet maximal speed and pausing fraction of transport were higher.
- Microtubule plus (+)-end extension imaging visualized microtubular growth at 0.12 μm/s and revealed that DCVs were transported faster in the anterograde direction.
- DCV transport slowed down upon presynaptic bouton approach, possibly promoting synaptic localization and cargo release.
- Our work provides a basis to extrapolate DCV transport properties determined in cultured neurons to the intact mouse brain and reveals novel features such as slowing upon bouton approach and brain state-dependent trafficking directionality.

Abstract Neuronal dense core vesicles (DCVs) transport many cargo molecules like neuropeptides and neurotrophins to their release sites in dendrites or axons. The transport properties of DCVs in axons of the intact mammalian brain are unknown. We used viral expression of a DCV cargo reporter (NPY-Venus/Cherry) in the thalamus and two-photon *in vivo* imaging to visualize axonal DCV trafficking in thalamocortical projections of anaesthetized and awake mice. We found an average speed of 1 μm/s, maximal speeds of up to 5 μm/s and a pausing fraction of ~11%. Directionality of transport differed between anaesthetized and awake mice. *In vivo* microtubule +-end extension imaging using MACF18-GFP revealed microtubular growth at 0.12 μm/s and provided positive identification of antero- and retrograde axonal transport. Consistent with previous reports, anterograde transport was faster (~2.1 μm/s) than retrograde transport (~1.4 μm/s). In summary, DCVs are transported with faster maximal speeds and lower pausing fraction *in vivo* compared to previous results obtained *in vitro*. Finally, we found that DCVs slowed down upon presynaptic bouton approach. We propose that this mechanism promotes synaptic localization and cargo release.

J. Knabbe and J. P. Nassal contributed equally to this work.

Knabbe J, Nassal JP, Verhage M & Kuner T (2018). Secretory vesicle trafficking in awake and anesthetized mice: differential speeds in axons *versus* synapses. *bioRxiv*. DOI: 10.1101/268078.

DOI: 10.1113/JP276022

(Received 18 February 2018; accepted after revision 24 May 2018; first published online 29 May 2018)
Corresponding author T. Kuner: Department of Functional Neuroanatomy, Institute for Anatomy and Cell Biology, Heidelberg University, Im Neuenheimer Feld 307, 69120 Heidelberg, Germany. Email: kuner@uni-heidelberg.de

Introduction

Neuronal dense core vesicles (DCVs) represent a diverse group of large secretory granules containing an electron-dense core as defined by electron microscopy. DCV cargo molecules differ between neuronal subtypes and include a variety of signalling molecules like neuropeptides, neurotrophic factors (such as BDNF), guidance cues, extracellular proteases and others. These signalling molecules are important for a variety of functions including synaptic plasticity, neurotransmission, neuronal development and survival (Huang & Reichardt, 2001; Samson *et al.* 2006; Cohen & Greenberg, 2008; van den Pol, 2012). Moreover, DCV cargos play important roles in several diseases such as social anxiety disorders (oxytocin and vasopressin) (Meyer-Lindenberg *et al.* 2011)), stress disorders (NPY) (Reichmann & Holzer, 2015) and neurodegenerative diseases such as Alzheimer's disease (Reichmann & Holzer, 2015). Despite their immense physiological and pathophysiological importance, we know very little about the biology of DCV trafficking in the intact mammalian brain.

DCVs are produced in the Golgi network (Kim *et al.* 2006) and transported via microtubule-dependent motor proteins (Zahn *et al.* 2004; Kwinter *et al.* 2009; Lo *et al.* 2011) towards their axonal or dendritic release sites. In contrast to synaptic vesicles, the content released by DCVs is not recycled locally, but degraded by membrane- or circulating metallo-endopeptidases (Rose *et al.* 2009). The highly dynamic transport of DCVs (Hartmann *et al.* 2001; de Wit *et al.* 2006; van de Bospoort *et al.* 2012; Wong *et al.* 2012; Farina *et al.* 2015; Gumy *et al.* 2017) ensures a reliable supply to often very distant locations in the axon and dendrites. Previous studies have shown an anterograde and retrograde cycling of DCVs through the axon with sporadic pauses in axonal *en-passant* boutons, also referred to as varicosities, which was concluded to represent an activity-dependent capture mechanism (Shakiryanova *et al.* 2006; Wong *et al.* 2012). The function of this mechanism is probably to enhance availability of DCVs at synapses to facilitate regulated secretion. The fusion of DCVs with the plasma membrane mostly occurs at/near synapses and can be induced with electrical high-frequency stimulation *in vitro* (Hartmann *et al.* 2001; de Wit *et al.* 2009; van de Bospoort *et al.* 2012). To date, it is not known if DCV transport *in vivo* is influenced by properties of the surrounding neuropil. Studies addressing DCV trafficking in the intact mammalian brain are lacking. The dense packaging of axonal and dendritic compartments within the neuropil could mechanically affect local trafficking conditions, in particular when considering that axons can have diameters of less than 100 nm (Berbel & Innocenti, 1988), about the size of one DCV. Furthermore, neuro-glial interaction could affect DCV trafficking. In addition to these factors, different functional states of the brain such as sleep or wakefulness may have an impact on the properties of DCV trafficking and release. On a cellular level, different patterns of spontaneous and evoked activity in neurons in the intact brain, known to be more extensive than typically present in cultured neurons or acute brain slices, could significantly affect DCV transport properties. Until now, DCV transport was only studied in neuronal cell culture and model organisms like *D. melanogaster* (Wong *et al.* 2012) and *C. elegans* (Zahn *et al.* 2004). Hence, to understand the contribution of aforementioned factors to DCV trafficking and to extrapolate published data obtained in reduced cell culture or brain slice preparations to living and behaving mammals, DCVs need to be imaged within the intact brain.

We established an *in vivo* DCV imaging approach using chronically implanted cranial windows and two-photon microscopy in anaesthetized and awake mice to describe the basic DCV transport characteristics in thalamocortical axons ramifying in the molecular layer of the primary motor cortex. We show that DCVs travel through thalamocortical axons *in vivo* with an average speed of 1 μm/s and maximal speeds of up to 5 μm/s with infrequent pauses. Furthermore, we show that DCVs preferentially slow down near presynaptic *en-passant* boutons. We propose this mechanism helps to promote synaptic localization and release of neuropeptides and neurotrophins.

Methods

Ethical approval

This study was carried out in accordance with the European Communities Council Directive (86/609/EEC) to minimize animal pain or discomfort. All experiments were conducted following the German animal welfare guidelines specified in the TierSchG. The local animal care and use committee (Regierungspräsidium Karlsruhe of the state Baden-Württemberg) gave approval for the study under the number G167/15. The authors declare that the reported experiments comply with *The Journal of Physiology*'s ethical principles and its checklist on animal experimentation. Male C57Bl/6N mice were acquired from Charles River Laboratories (Sulzfeld, Germany) at an age of 8 weeks. The mice were kept at a 12—12 h

dark–light cycle synchronized with the local day–night cycle. Water and food were available *ad libitum*, except for the imaging sessions. Mice were generally housed in ventilated racks with up to 3 animals per cage, but were separated after surgery to minimize the risk of injury. After completion of the experiments, mice were killed with an overdose of Narcoren (Merial GmbH, Hallbergmoos, Germany; 500 mg kg^{-1} bodyweight I.P.).

Immunohistochemistry

For immunohistochemistry, mice were deeply anaesthesised with Narcoren (500 mg kg^{-1} bodyweight I.P.) and transcardially perfused with 4% paraformaldehyde (PFA) in phosphate-buffered saline (PBS). The brains were post fixed overnight in 4% PFA and then sliced into 70 μm thick sections and stored in PBS. For increased permeabilization, the slices on which the chromogranin stains were performed on, were treated with 1% sodium dodecyl sulfate (SDS) in PBS for 5 min before the antibody stainings. For antibody staining the slices were incubated for 1 h in PBS containing 5% normal goat serum (NGS), 1% bovine serum albumin (BSA), 1% cold fish gelatin and 0.5% Triton X-100. Incubations with primary antibodies were done overnight at 4°C. The secondary antibodies were incubated for 1–2 h at room temperature. Primary antibodies were: Bassoon (Enzo Life Sciences, SAP7F407; 1:1000, RRID:AB_2313990), chromogranin A (Synaptic Systems, Göttingen, Germany, 259003; 1:500, RRID:AB_2619972), chromogranin B (Synaptic Systems, 259103, 1:500, RRID:AB_2619973), early endosomal antigene 1 (Eea1) (Abcam, Cambridge, UK; ab2900; 1:200, RRID:AB_2262056), Homer1 (Synaptic Systems, 160003; 1:200, RRID:AB_887730), Lamp-2 (Santa Cruz Biotechnology, Heidelberg, Germany, sc-18822; 1:200, RRID: AB_626858, kind gift from Ralph Nawrotzki), LC-3 (Medical & Biological Laboratories, Nagoya, Japan, M-152-3; 1:100; RRID:AB_1279144, kind gift from Ralph Nawrotzki), Piccolo (Synaptic Systems, 142104; 1:1000, RRID:AB_2619831), Rab5 (Abcam, ab18211; 1:200, RRID: AB_470264, kind gift from Ralph Nawrotzki). Alexa Fluor antibodies from Invitrogen were used as secondary antibodies in a dilution of 1:500. The slices were mounted in SlowFade Gold (Life Technologies) and imaged on a Leica SP8 inverted confocal microscope with a 63× oil immersion objective (NA = 1.4) and maximal resolution in x, y and z planes (0.08 μm × 0.08 μm × 0.3 μm).

Genetic labelling of DCVs and thalamo-cortical axons using viral gene transfer

DCVs were labelled *in vivo* in mice by viral expression of a fusion protein consisting of Neuropeptide Y (NPY) and the yellow fluorescent protein Venus (NPY-Venus) (Fig. 1*A* and *B*) or the red fluorescent protein mCherry (van de Bospoort *et al.* 2012; Farina *et al.* 2015), driven by the synapsin promoter. Axonal projections were labelled by expressing mCherry under the control of the CAG (chicken-beta-actin) promoter in thalamic projection neurons. Microtubule plus (+)-ends were marked by expression of green fluorescent protein (GFP) fused to the first 18 N-terminal amino acid residues of the microtubule +-end marking protein MACF43 fused to the two-stranded leucine zipper coiled-coil sequence corresponding to GCN4-p1 under control of the synapsin promoter as described elsewhere (Yau *et al.* 2016) (GFP-GCN4-MACF18). Recombinant adeno-associated virus (AAV) particles of the chimeric 1/2 serotype were produced with the plasmids described above (Schwenger & Kuner, 2010).

Craniectomy, stereotaxic injection and chronic window implantation

For viral injection (Wimmer *et al.* 2004) and craniectomy (protocol adapted from Holtmaat *et al.* 2009), mice were anaesthetized with an intraperitoneal (I.P.) injection of a mixture of 0.48 μl fentanyl (1 mg/ml; Janssen), 1.91 μl midazolam (5 mg/ml; Hameln) and 0.74 μl medetomidin (1 mg/ml; Pfizer) per gram body weight each and placed in a stereotaxic head holder (Kopf). Depth of anaesthesia was monitored by checking for vibrissal movements, breathing frequency and pain reflexes. Before cutting of the skin, xylocaine solution (1%; Astra Zeneca) was injected subcutaneously. A small hole in the skull was made with a dental drill over the injection site. Then, 1 μl of a 1:1 mixture of the NPY-Venus and mCherry or a mixture of MACF-GFP and NPY-mCherry AAV particles was slowly injected into the right medio-dorsal thalamus (Coordinates from bregma: $x = 1.13$, $y = -0.82$, $z = -3.28$). Afterwards a circular craniectomy (approx. 6 mm, centre positioned 1 mm right of bregma) was drawn with a dental drill. The dura was carefully removed. A sterile round no. 0 coverslip with a diameter of 6 mm (cranial window) and a custom-made round plastic holder surrounding it for head fixation were cemented on the skull with dental acrylic (Hager & Werken).

After surgery, mice received I.P. a mixture of 1.86 μl naloxon (0.4 mg/ml; Inresa), 0.31 μl flumazenil (0.1 mg/ml; Fresenius Kabi), 0.31 μl antipamezole (5 mg/ml; Pfizer) in 3.72 μl saline (0.9%; Braun) each per gram body weight to antagonize the anaesthesia. Mice were given carprofen (Rimadyl, 5 mg/kg; Pfizer) in saline before surgery and during the following days in intervals of 12 h for 3 days. Mice were single housed after surgery and typically imaged at least 21 days after

the surgery. This waiting period is essential for the glial reaction below the window to subside (Holtmaat *et al.* 2009).

In vivo two-photon imaging

Two-photon imaging of small structures like DCVs provides a challenge that is illustrated in Fig. 1*C* and *D*. A DCV positioned anywhere within the focal volume will result in a similar signal. Single labelled DCVs compete with background autofluorescence signals (blue filled circles, Fig. 1*C*). To be detectable, the fluorescence signal arising from the DCV will have to exceed the number of autofluorescence signals present in the background. DCVs located outside the focal volume will not be detected. Figure 1*D* illustrates the presence of two axons within

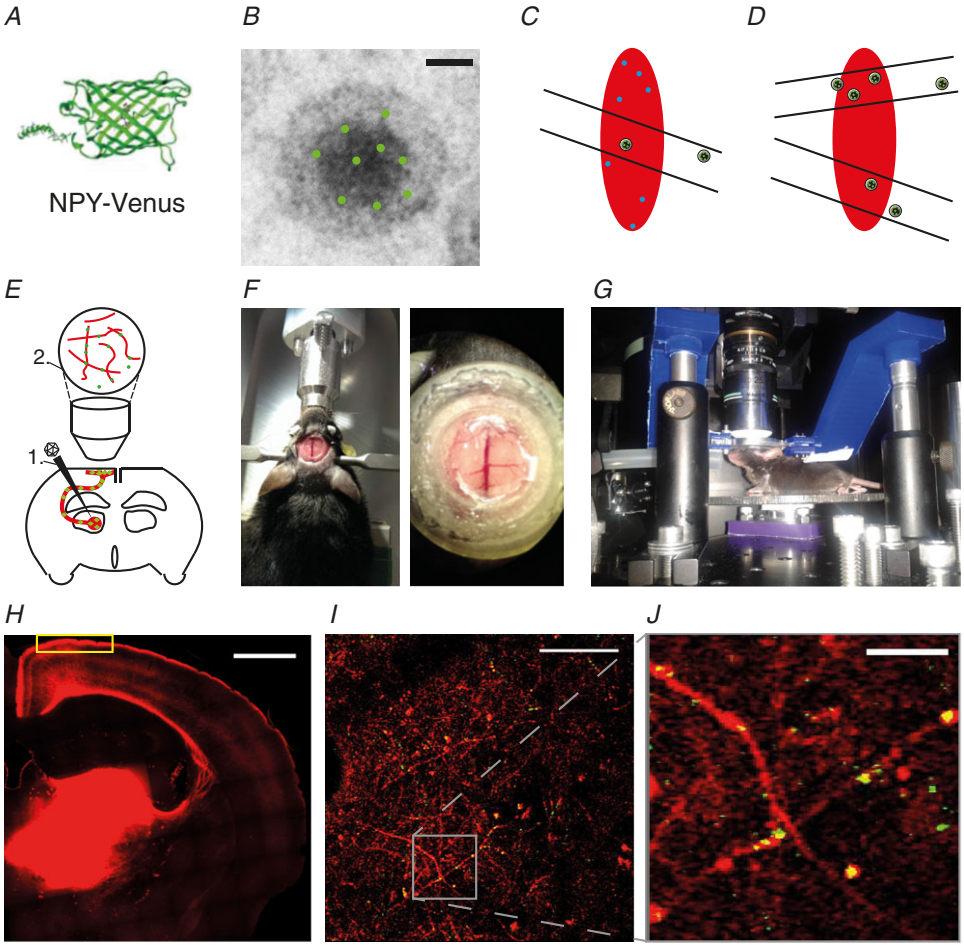

Figure 1. Experimental design
A, NPY-Venus shown as an approximated molecular model to clarify the relative size of the components of the fusion protein. *B*, EM image of a DCV with an arbitrary number of NPY-Venus molecules (green) to illustrate the DCV labelling strategy. Scale bar, 20 nm. *C*, the red oval shape represents the illuminated focal volume of two photon excitation (approximated from the point-spread function). Lines illustrate an axon positioned within the focal volume. Blue dots denote background fluorescence. *D*, situation illustrating the presence of two axons and multiple DCV within a single focal volume (see Methods section for further discussion). *E*, injection of AAVs encoding NPY-Venus and mCherry into the area of the right medio-dorsal thalamus (1). Position of objective for imaging (2). Note the orientation of superficial axons in parallel to the brain surface. *F*, chronic window implantation after stereotaxic delivery. *G*, setup for awake imaging. The mouse is fixed via the crown, but able to move on a freely rotatable disc. *H*, mosaic scan of thalamic injection site and axonal projection emanating from it (wide-field epifluorescence imaging of an 80 μm thick section; scale bar, 1 mm). Yellow rectangle depicts region of interest imaged in primary motor cortex, 30–80 μm below the pial surface. *I*, example image of a single frame used for *in vivo* two-photon time-lapse imaging 40 μm below the pial surface. mCherry-labelled axons (red) and NPY-Venus-labelled DCVs (green), DCVs in labelled axons appear yellow. Scale bar, 50 μm. *J*, magnified view of region marked in *I*. Scale bar, 10 μm.

a single focal volume, making it impossible to assign the total fluorescence recorded to the individual axons. Hence, imaging requires a low density of axons within the imaging volume. Multiple DCVs placed within the same axon and focal volume will be detected as a single, yet brighter, fluorescence spot. If these DCVs move together, it will be difficult to precisely identify the number of DCVs within that cluster.

Two-photon imaging (Denk *et al.* 1994) was performed with a TriM Scope II microscope (LaVision BioTec GmbH) equipped with a pulsed Ti:Sapphire laser (Chameleon; Coherent). 960 nm was used for simultaneous excitation of both Venus and mCherry. For the experiments with MACF-GFP and NPY-mCherry, a wavelength of 995 nm was used. Imaging was performed with a 25× water immersion objective (Nikon MRD77225, NA = 1.1) and appropriate filter sets (Venus: 535/70 nm and mCherry: 650/100; Chroma). Fluorescence emission was detected with low-noise high-sensitivity photomultiplier tubes (PMTs, H7422-40-LV 5M; Hamamatsu). For the imaging sessions, anaesthesia was induced with 6% isoflurane (Baxter) in oxygen and maintained at 0.8–1%. Depth of anaesthesia was monitored by checking for vibrissal movements, breathing frequency and pain reflexes. The anaesthetized mouse was head fixed by clamping the plastic holder cemented to the skull. For awake imaging, the mouse was fixed over a rotatable disc treadmill (Fig. 1*G*) under isoflurane anaesthesia and the isoflurane was shut off after fixing. The awake imaging was started at least 5 min after the end of isoflurane anaesthesia. Frames were typically taken from an area of 196.6 × 196.6 μm at 1024 × 1024 pixel resolution with a frame rate of 1.06 Hz for 10 min per dataset using the galvanometric scanner of the TriM Scope II. Anaesthetized imaging sessions lasted no longer than 1 h and awake imaging sessions no longer than 20 min.

Processing and analysis of imaging data

The acquired movies were registered for image movement in the *x*–*y* plane with the Fiji (RRID:SCR_002285) Plugin 'Descriptor based series registration' (Preibisch *et al.* 2010). Generally, during anaesthetized imaging sessions, resulting displacement in *x*–*y* was less than 10 μm. The resulting stacks were deconvolved using the Richardson-Lucy algorithm implemented in Matlab (RRID:SCR_001622) and a theoretical PSF, background subtracted and median-filtered. To only analyse moving particles, the average projection of the registered time lapse was subtracted from every image. For the semi-automated tracking of the DCV puncta the Fiji Plugin 'Trackmate' (Tinevez *et al.* 2016) was used. The automatically tracked parts were manually reviewed. The tracks were stopped when the puncta were not visible for more than two images. The resulting coordinates in *x*, *y* and *t* (time) were analysed with custom written Matlab scripts. Only tracks exceeding 10 consecutive images were analysed. The maximal speed per track was defined as highest mean of the speed out of 4 consecutive track points. The mean speed was averaged over all computed mean speeds of all tracks. The unidirectionality factor was defined as the fraction of the puncta moving in the direction of the main movement vector as defined by the first and last track point. To calculate this, each movement episode of all puncta present in the axon was classified to be forward or reverse with the unidirectionality factor defined as number of forward movements/number of reverse movements. Hence, an unidirectionality factor of 1 corresponds to a consistent movement of puncta in one direction while values below 1 indicate that some of the puncta also moved in the opposite direction. A value of 0.5 would indicate that the same number of puncta moved forward and reverse, suggesting no preferential movement direction.

The MACF18-GFP comets were analysed using kymographs. Lines fitted over tracks in the kymographs were analysed with an ImageJ macro written by Alessandro Moro which uses a kymograph plugin (Bioimaging and Optics Platform) (Seitz & Surrey, 2006).

Statistics

All statistics were calculated using Prism (GraphPad, RRID:SCR_002798). Normality distribution of the data was tested using Kolmogorov-Smirnov, D'Agostino-Pearson and Shapiro-Wilk tests. Most analysed data did not show a gaussian distribution. Hence, distributions of the datasets were compared with non-parametric two-sided Mann-Whitney tests. A P value below 0.05 was considered statistically significant. Means reported in the text are given with the standard error of the mean (SEM) unless noted otherwise.

Results

To image DCVs *in vivo*, vesicles and axons were fluorescently labelled with NPY-Venus (Fig. 1*A*–*D*; see Methods for detailed discussion), a previously optimized DCV reporter (de Wit *et al.* 2009), and mCherry, using viral gene transfer into the right medio-dorsal thalamus (Fig. 1*E*). Thalamo-cortical projection neurons were chosen as a model system, because their axons branch intracortically in the superficial layer 1 and run parallel to the surface of the brain, thereby providing ideal conditions for DCV imaging. Chronically implanted cranial windows (Fig. 1*F*) permitted *in vivo* two photon microscopy in anaesthetized or awake mice (Fig. 1*G*)

(Holtmaat *et al.* 2009). Three weeks after viral injection and chronic window insertion, imaging commenced using 960 nm excitation for simultaneous visualization of axons and labelled DCVs. The thalamic injection site and mCherry-labelled axonal projections reaching the surface of the brain are schematically indicated in Fig. 1*H*, with the yellow rectangle indicating an area situated 30–80 μm below the pial surface, from which time-lapse data were acquired. An example of an *in vivo* two-photon imaging experiment is shown in Fig. 1*I*, illustrating that labelling of thalamocortical axons with mCherry allowed detection of axons positioned within a single imaging frame, an important precondition to monitor moving DCVs (yellow dots in Fig. 1*J*, Supporting Movie S1). The signal of analysed vesicles shows a mean signal to noise ratio between 2:1 and 4:1 as measured by the mean fluorescence of the vesicle divided by the background, thus providing reliable imaging conditions.

The time-lapse movies regularly showed large static fluorescent clusters that did not overlap with the mCherry labelled axons. These might represent either cellular autofluorescent debris or released fluorescent cargo of the DCVs that has been taken up by cells, possibly astrocytes or microglia. Co-staining for an astrocytic marker and a marker of early endosomes demonstrated an overlap of a portion of this fluorescent cargo and astrocytic early endosomes (data not shown).

To control for the correct packaging of the DCV cargo reporter, NPY-Venus, into DCVs under *in vivo* conditions, we immunostained fixed brain slices with the endogenous DCV markers chromogranin A and B (Chr-A, Chr-B). NPY-Venus-labelled DCVs were detected in mCherry-labelled axons and overlapped with Chr-A and Chr-B stainings (Fig. 2*A* and *B*). We found no overlapping fluorescent signals of NPY-Venus puncta with other cellular structures such as endosomes, lysosomes, autophagosomes or presynaptic proteins (Fig. 2*C*–*H*). To exclude that expression of the DCV cargo reporter induced the formation of DCVs in cells that may not *a priori* produce DCVs, we labelled thalamic axons with mCherry and immunostained for Chr-A (data not shown). This experiment demonstrates the presence of DCVs in thalamocortical axons independent of the NPY-Venus expression. In summary, these results suggest that the DCV cargo reporter NPY-Venus correctly labelled DCVs in neurons that endogenously produce DCVs, consistent with previous observations made in cultured neurons (Taraska *et al.* 2003; Farina *et al.* 2015).

Visualizing DCV movement in axonal projections *in vivo*

DCV trafficking in thalamocortical axons was monitored by time-lapse imaging of DCV reporter fluorescence and axonal fluorescence in single focal planes at 1 Hz. Individual DCV puncta can be assigned to the axons they are travelling in (Fig. 3*A*) and subsequently tracked (Fig. 3*B*). Small fluctuations in the apparent size of the puncta along the trajectory may arise from axons not running perfectly in parallel to the imaging plane, so that different amounts of fluorescent proteins in the vesicles are excited (see Fig. 1*C* and *D*). Alternatively, changes in the *z* focus position in response to slight movements of the tissue may account for fluctuations in apparent size of the puncta. The average length of axonal segments analysed was 30 ± 10 μm and time-lapse movies lasted for typically 10 min. At $t = 2$ s, the DCVs marked yellow and blue in Fig. 3*B* appear to travel within the same diffraction-limited focal volume. Such co-travelling events were encountered only rarely (on average less than once in each kymograph of 51 axon stretches analysed). During the time period from 2 s to 14 s, the puncta labelled green and orange travel with different speeds (1.6 μm/s; 0.6 μm/s) in the same direction. This is further illustrated in the kymograph (Fig. 3*C*). Hence, tracing of labelled DCVs can be achieved with the approach introduced here, including quantitative analyses.

Quantification of DCV trafficking characteristics *in vivo*

Following the experimental scheme shown in Fig. 1, a total of 279 vesicles in eight mice were tracked semi-automatically. The average speed of moving DCV puncta *in vivo* in anaesthetized mice was 1.03 ± 0.03 μm/s (Fig. 4*A* and *J*). This is in agreement with previous observations in cultured mammalian neurons and with *in vivo* imaging performed in *D. melanogaster*, ranging from speeds of 0.75 μm/s to 1.25 μm/s for axonal DCV transport (see coloured points in Fig. 4*A*) (de Wit *et al.* 2006; Kwinter *et al.* 2009; Bittins *et al.* 2010).

The maximum speed per track was defined as the highest average speed within 4 consecutive track points of each track. The average maximum speed of the tracked vesicles was 2.06 ± 0.05 μm/s (Fig. 4*B*), but we regularly observed speeds of up to 5 μm/s (*in vitro* data: 2.6 μm/s to 3.75 μm/s; de Wit *et al.* 2006; Bittins *et al.* 2010).

DCV puncta often slowed down and stopped, but started moving again at a later time point (pausing). The pausing time was defined as the percentage of time that a punctum moved slower than 0.2 μm/s. This corresponds roughly to a displacement of one pixel per image. The overall pausing time of the tracked vesicles was 10.7 ± 0.7% (Fig. 4*C*). This is lower than the 22% pausing fraction reported in cell culture (de Wit *et al.* 2006).

It was not possible to determine whether DCV puncta moved in the anterograde or retrograde direction within the axon, because the position of the soma could not be

determined *in situ*. To analyse if vesicles moved back and forth, or if they followed a preferred movement vector, the directionality factor for the overall movement of a vesicle was calculated. This 'unidirectionality factor' was defined as the fraction of time the vesicle moved along its overall directional vector defined by the first and last point of the track. The mean unidirectionality factor of all 279 analysed tracks is 0.86 ± 0.01 (Fig. 4*D*). This corresponds to an overall consistent unidirectional movement of the puncta. The remaining 14% of movements were in the opposite direction to the main movement vector.

To compare the amount of bidirectional and unidirectional movement in individual axons, only axons with more than 5 tracked puncta were investigated to avoid a possible bias towards unidirectional movement. In total, 25 axons were analysed. The frequency distribution of the directionality in these axons shows that in approximately 40% of the axons DCVs move only in one direction (Fig. 4).

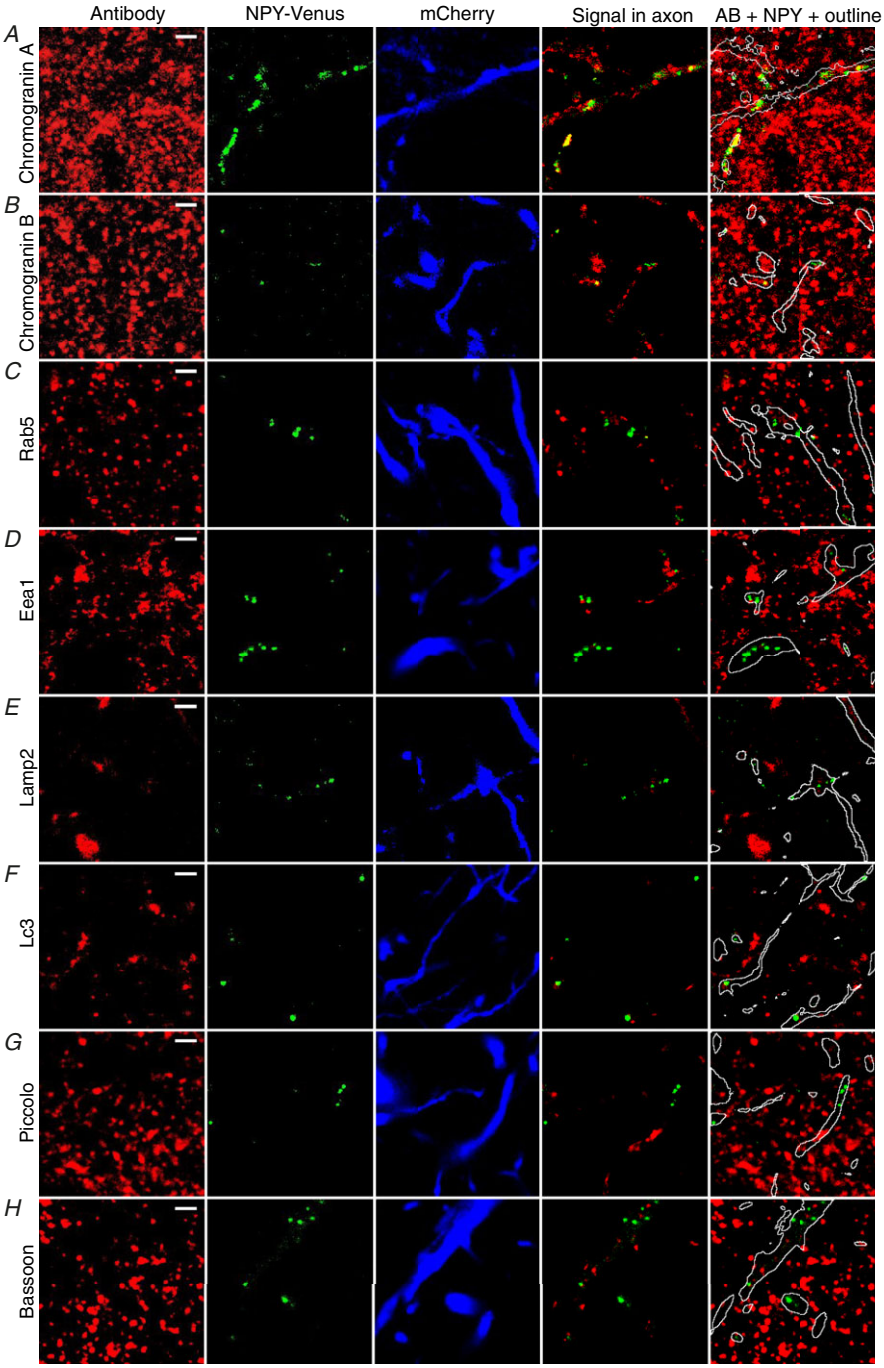

Figure 2. Verification of DCV identity
A–H, average intensity projections of 5 consecutive confocal image planes of immunostained cortical tissue sections with NPY-Venus-labelled DCVs (green) and mCherry-labelled axons (blue). Colocalization of the respective antibody with DCVs within labelled axons is shown in the fourth column (Signal in axon), all signals outside of labelled axons omitted. The fifth column shows the respective antibody staining and labelled DCVs, with labelled axons outlined (AB + NPY + outline). *A* and *B*, antibody stainings against DCV markers chromogranin A and chromogranin B. *C–F*, antibody stainings against mobile compartments: endosomes (Rab5, Ras-related protein 5a; Eea1, early endosome antigen 1), lysosomes (Lamp2, lysosome-associated membrane protein 2), autophagosomes (Lc3, microtuble-associated protein light chain 3). *G* and *H*, antibody stainings against presynaptic active zone proteins: Bassoon, Piccolo. Scale bars, 2 μm.

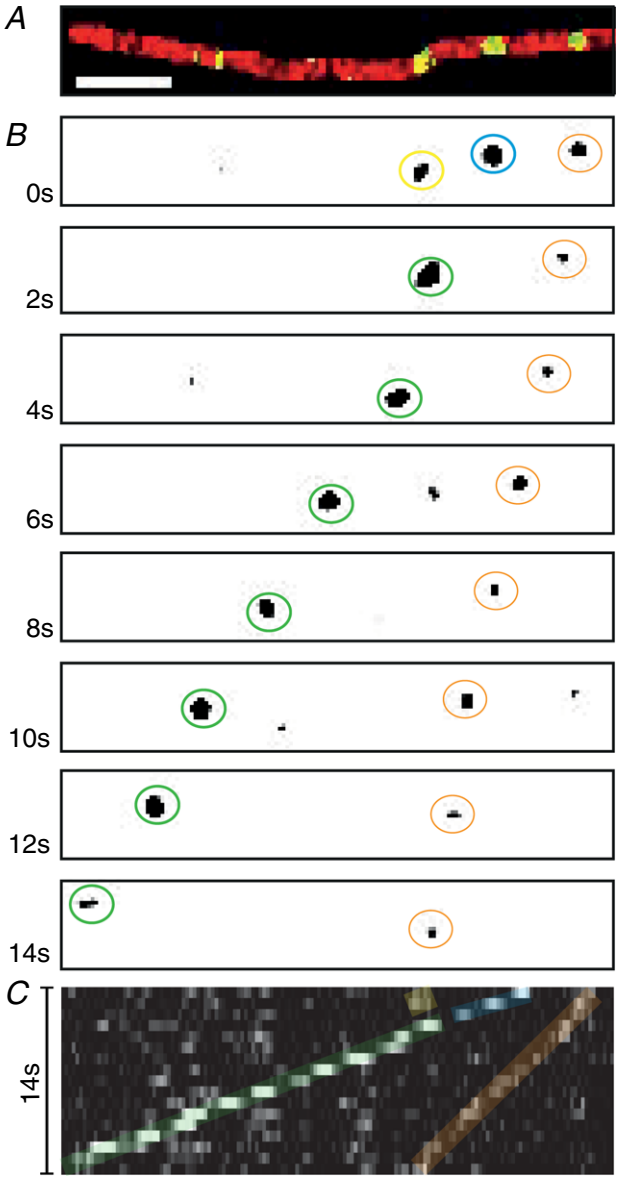

Figure 3. Time-lapse images and kymograph of moving DCVs in a single axon
A, single two-photon image frame showing an axon labelled with mCherry (red) and the DCV cargo reporter NPY-Venus (green). Scale bar, 5 μm. *B*, time-lapse images of the green channel in panel *A*. DCVs labelled blue and yellow at $t = 0$s travel together (green) in subsequent frames. *C*, kymograph of time-lapse in *B*.

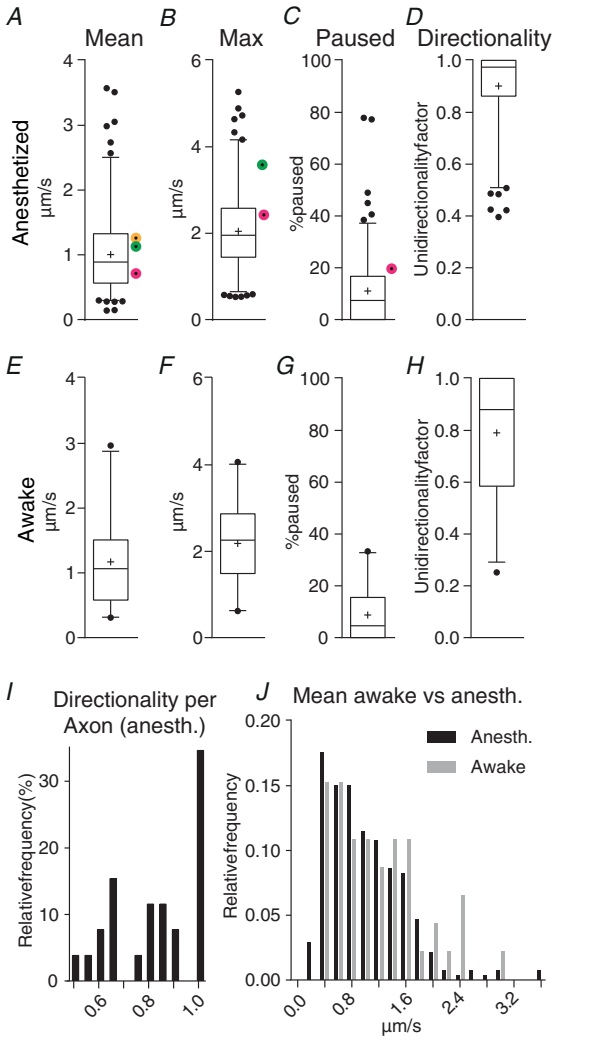

Figure 4. DCV movement dynamics resemble previous *in vitro* studies
A–D, box plots of 279 tracked puncta taken from 8 anaesthetized mice. Box plots show the median and the 25 to 75 percentile, the whiskers show the 2.5 to 97.5 percentiles. Individual points above or below the whiskers are outliers. Coloured points represent previous reported data from *in vitro* studies. Magenta dots, de Wit *et al.* 2006 (experiments performed at 32°C); green dots, Bittins *et al.* 2010; yellow dots, Kwinter *et al.* 2009 (experiments performed at 37°C). *B*, maximal speed averaged over 4 consecutive track points. *C*, pausing time as the percentage of images in which puncta moved with a speed below 0.2 μm/s. *D*, directionality of all vesicles. *E–H*, puncta tracked in awake mice ($n = 46$ puncta, 3 mice). No significant differences (Mann-Whitney test) were found for mean speed ($P = 0.12$), maximal speed ($P = 0.28$), and fraction paused ($P = 0.22$), while the directionality differed highly significantly ($P = 0.0001$). *I*, distribution of directionality of transport in axons with $n > 4$ tracked vesicles. *J*, frequency distributions of mean speeds in awake (black bars) and anaesthetized (grey bars) mice.

Bidirectional movement was observed in approximately 60% of the axons.

To test possible confounding effects on the trafficking characteristics due to different expression time and thus different amounts of DCV cargo reporter expressed, two mice were imaged twice, at 2–3 weeks and 8–9 weeks after viral injection (data not shown). No significant differences in the transport speeds and other trafficking characteristics of the NPY-Venus puncta were found between these time points, suggesting that the amount of reporter expressed did not affect the trafficking properties of DCVs.

In summary, the basic DCV trafficking properties were similar in the anaesthetized intact brain in

comparison to a large set of trafficking data previously described in neuronal cell cultures. However, *in vivo,* the peak speed was higher and the pausing time lower.

Comparison of DCV trafficking in anaesthetized and awake mice

To control for potential influence of anaesthesia, and thus brain activity levels in general, on DCV transport, three mice were imaged in the awake state. Minor axial movements exceeding 1–2 μm remove the axon stretch of interest from the imaging plane (see Fig. 1*C* and *D*). Therefore, the base plate of the window was firmly fixed, both on the skull and in the holder, while placing the mouse on a rotatable disk (Fig. 1*G*). The axial focal plane remained stable, except when the mice started to run. These episodes were excluded from further analysis. Forty-six tracks in awake and resting mice were analysed and trafficking characteristics from these tracks were compared to all tracks recorded from anaesthetized mice. The mean speed of DCV puncta was 1.17 $\pm$ 0.1 μm/s in the awake state and did not differ from the mean speed of 1.03 $\pm$ 0.03 μm/s in anaesthetized mice (Fig. 4*E*, Supporting Movie S2). This is further illustrated by the large overlap of the frequency histograms of both distributions (Fig. 4*J*). The maximal speed and pausing time did not differ significantly between anaesthetized and awake mice (Fig. 4*F* and *G*).

The only feature in DCV trafficking that was significantly different in the awake compared to anaesthetized mice was the lower directionality factor of 0.79 $\pm$ 0.03 in awake animals compared to 0.9 $\pm$ 0.01 (Mann-Whitney test, $P = 0.0002$) in anaesthetized animals (Fig. 4*H*). This could potentially be explained by interfering movement of the animal that could not be corrected for during recordings. However, intrinsic differences caused by the activity state of the brain may also affect DCV movement directionality, leading to less straightforward tracks with more pausing and reversing of the movement direction.

Axonal microtubule dynamics *in vivo*

To differentiate between anterograde and retrograde DCV trafficking *in vivo*, we co-expressed NPY-mCherry and MACF18-GFP, a minimal fragment of the microtubule-actin cross-linking factor 2 that gets selectively incorporated at the microtubule +-end (Yau *et al.* 2016). This allowed us not only to determine axonal orientation for trafficking analysis but also to characterize axonal microtubule growth dynamics. MACF18-GFP fluorescence accumulated at the growing microtubule plus ends are referred to as comets (Fig. 5, Supporting Movie S3). As overexpression of MT-plus end binding proteins can lead to the binding to all microtubules and not only the plus ends (Komarova *et al.* 2005), we analysed these mice exclusively after 3–4 weeks of expression time, where punctate fluorescent and only faint cytoplasmic signals could be observed in axons. Analysis of the kymographs of MACF18-GFP comets allowed us to quantify movement speeds of axonal microtubules *in vivo*; 155 comets in 17 axons of four mice were analysed. We found a mean speed of axonal microtubule polymerization *in vivo* of 0.12 $\pm$ 0.01 μm/s (Fig. 5*D*). This is in agreement with *in vivo* findings in spinal cord axons of 0.147 μm/s (Kleele *et al.* 2014). The average run length of single comets was 10.02 $\pm$ 0.59 μm (Fig. 5*E*). To compare the number of comets per axon stretch length and time to previously reported numbers, we calculated the number of comets per micrometer (μm) per minute (Fig. 5*F*). With ~0.4 comets/min/20 μm (~0.02 comets/min/μm) we observed fewer comets than the previously reported number of ~1.8 comets/min/20 μm (Yau *et al.* 2016) in dendrites. We found a density of 0.028 $\pm$ 0.0002 comets/μm which is in the range of the data reported by Kleele *et al.* (2014) in spinal cord axons (0.033 $\pm$ 0.002 comets/μm).

Anterograde *versus* retrograde DCV trafficking

Assessing the run direction of MACF18-GFP puncta allowed us to define the directionality of DCV movement within the same axon as anterograde or retrograde with respect to the soma. The unidirectional movement of multiple microtubule comets (green) within a single axon stretch define the orientation of this axon: anterograde corresponds to movement from left to right in the kymograph (Fig. 6*A*). The movements of multiple DCVs in the same axonal stretch (red) reveal their dynamic bidirectional transport.

In the axons the mean speed of DCV transport in the anterograde direction was 2.14 $\pm$ 0.12 μm/s ($n = 78$) and in retrograde direction 1.4 $\pm$ 0.08 μm/s ($n = 67$; Fig. 6*B*). This analysis showed a significant difference in transport speed (Mann-Whitney test, $P < 0.0001$). Additionally, we compared mean speeds of anterograde and retrograde transport within axons (with $n > 2$ vesicles in each direction). In almost all axons, the anterograde vesicles were faster than the retrograde vesicles (Fig. 6*F*). The maximum speed, pausing time and unidirectionality factor showed significant differences in the antero- and retrograde trafficking directions (Fig. 6*C*–*E*). Thus, *in vivo* imaging revealed a difference in anterograde and retrograde trafficking speed comparable to that previously published in cultured neurons (de Wit *et al.* 2006) and invertebrates (Zahn *et al.* 2004; Barkus *et al.* 2008).

DCV trafficking is different near axonal boutons *in vivo*

While analysing the tracking data, we noticed that some of the axons showed different trafficking features at sites that resembled *en-passant* boutons, visible as ellipsoid structures with a diameter of 2–4 μm (Fig. 7*A*, red). To confirm that these structures correspond to axonal boutons, we performed immunostainings for the pre- and postsynaptic markers synaptophysin and Homer1, respectively. NPY-Venus puncta overlapped with synaptophysin-positive puncta within ellipsoid structures of the axon (Fig. 7*B*) and were associated with Homer1-positive puncta nearby (Fig. 7*C*), indicating that the ellipsoid structures of typical size and shape represent presynaptic boutons.

Each of the boutons shown in Fig. 7*A* contains DCV puncta that turned out to be immobile or mobile (Fig. 7*D*, orange *versus* red circles). Upon passing the bouton, mobile puncta slow down near the boutons (red, see also trajectory in kymograph, Fig. 7*E*). For the subsequent analysis, 57 tracks of axons with visible boutons from three mice were compared to tracks in axons lacking boutons. The average speed of DCV puncta was significantly lower in the axons containing boutons with a difference of 0.3 μm/s (Fig. 7*F*; bouton: 0.78 $\pm$ 0.11 μm/s; non-bouton: 1.10 $\pm$ 0.03 μm/s; MW: $P < 0.0001$). The maximal speed was significantly lower too, with a difference of 0.3 μm/s (Fig. 7*G*; bouton: 1.81 $\pm$ 0.16 μm/s; non-bouton: 2.16 $\pm$ 0.05 μm/s; MW: $P < 0.0001$). The pausing time of the vesicles was different, with a higher fraction of pausing vesicles in/around boutons (Fig. 7*H*; bouton: 20.43 $\pm$ 2.14%; non-bouton: 8.50 $\pm$ 0.61%; MW: $P < 0.0001$). Finally, changes in movement directionality were increased in axons containing boutons (Fig. 7*I*, 0.79 $\pm$ 0.02; non-bouton: 0.90 $\pm$ 0.01; MW: $P < 0.0001$).

To investigate further at which distance from the bouton center the reduction in speed occurred, all bouton centre points were marked manually. Mean speeds of tracks outside a certain distance from the centre were analysed covering a range of 1 to 10 μm (Fig. 7*J*). A steady decrease in mean speed from $\sim$ 0.9 μm/s to $\sim$ 0.5 μm/s occurred within a distance of 10 μm towards the bouton centre. We conclude that a lower mean speed of vesicles within and near boutons leads to longer residence of trafficking DCVs in presynaptic boutons, facilitating the recruitment of DCVs for secretion in synaptic boutons.

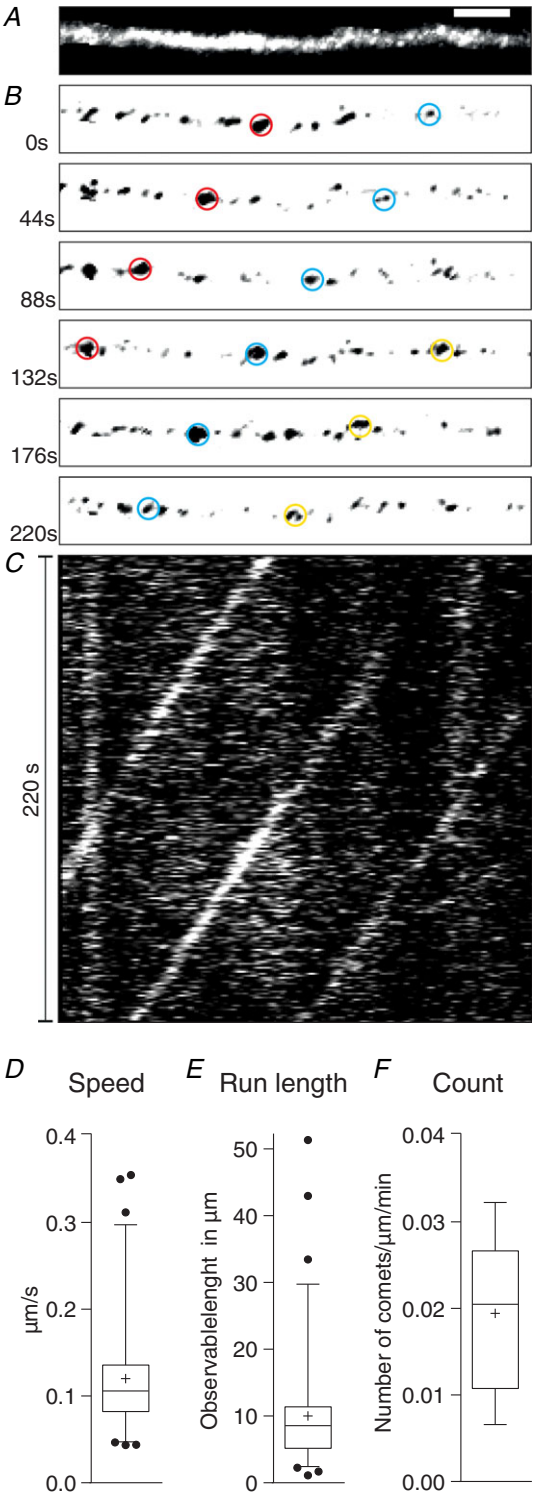

Figure 5. Axonal microtubule dynamics *in vivo*
A, maximum intensity projection of time-lapse of MACF18-GFP positive, manually segmented axonal stretch. Scale bar, 5 μm. *B*, time-lapse of microtubule +-end growth. Three comets are marked with coloured circles. *C*, kymograph of time-lapse shown in *B*. *D–F*, box plots of mean speed, run length and number of comets per minute per micrometer (μm).

Discussion

We characterized DCV trafficking dynamics in anaesthetized and awake mice in axons of thalamo-cortical projection neurons. Our experimental protocol allows

imaging of fluorescently labelled neuronal DCVs through chronic cranial windows in mice, transferring basic cell biology from the culture dish to the more complex and realistic environment of higher order systems. While many axonal DCV trafficking properties previously described *in vitro* are similar to those revealed here *in vivo*, we found a higher peak transport speed, a lower fraction of pausing DCVs and a slow-down of DCV trafficking upon approach to axonal boutons. The latter is consistent with a preferential capture and release of DCVs at presynaptic sites in the anaesthetized and awake mouse brain.

NPY-Venus-labelled punctate structures showed the trafficking features of DCVs and were confirmed as such using staining for chromogranin A/B (Fig. 2*A* and *B*). Furthermore, NPY-Venus signals did not overlap with other (mobile) organelles such as endosomes, lysosomes or autophagosomes, or presynaptic proteins (Fig. 2*C–H*). Together, these observations strongly indicate that NPY-Venus-labelled structures represent DCVs. The NPY-Venus puncta travelling through axons had different sizes and fluorescence intensities, suggesting that puncta may consist of either single or multiple DCVs (Figs 1*J*, 3 and 7), consistent with published *in vitro* data (van de Bospoort *et al.* 2012). It has been argued that thalamocortical and pyramidal cortical neurons lack DCVs altogether (Torrealba & Carrasco, 2004), although thalamic projection neurons have not been systematically investigated for DCVs. By selectively labelling thalamic projection neurons with mCherry and performing stainings of the endogenous DCV marker chromogranin A, we could demonstrate that DCVs naturally occur in these neurons. Hence, NPY-Venus

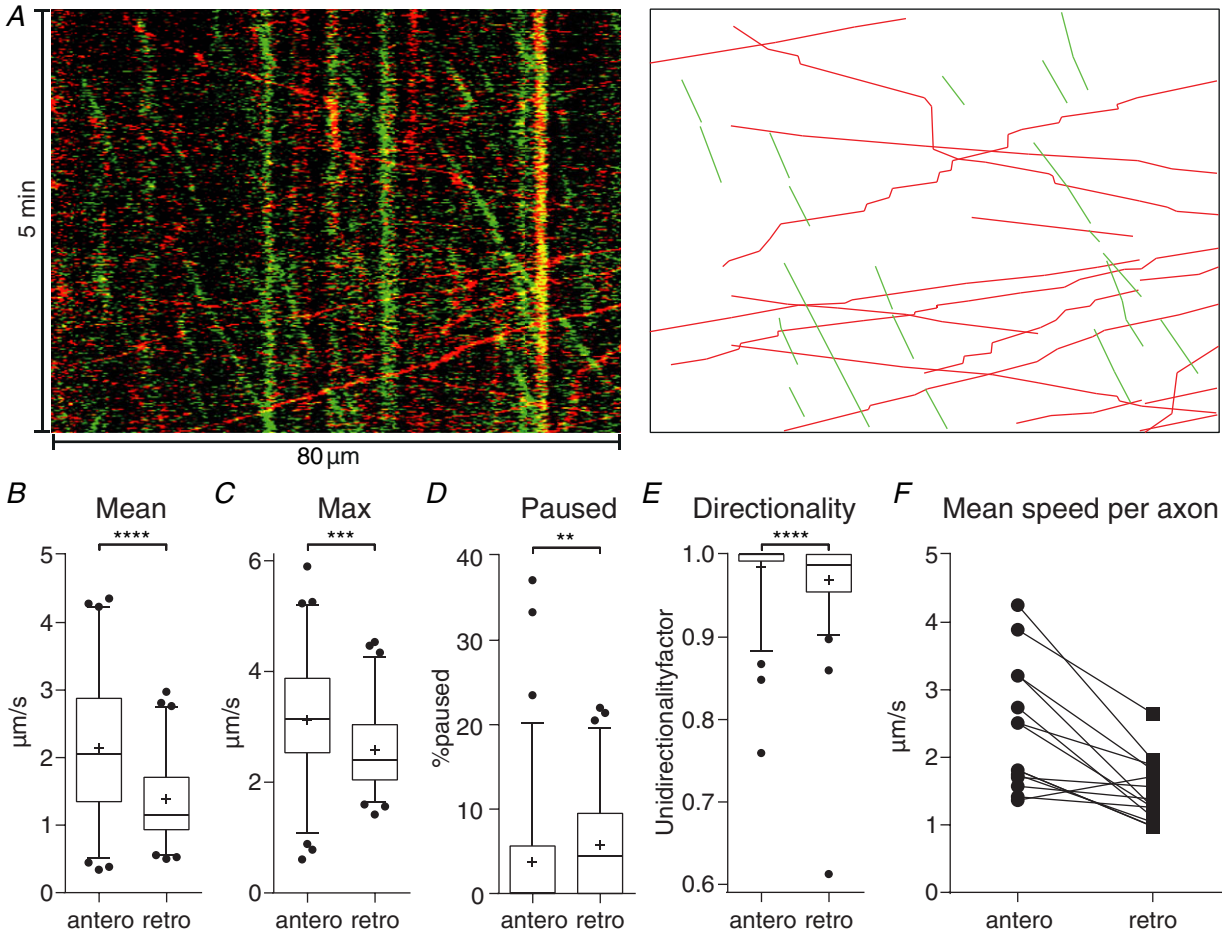

Figure 6. Anterograde *versus* retrograde trafficking of DCVs *in vivo*
A, left, kymograph covering 5 min of an axon stretch with green puncta depicting MACF18-GFP comets and red puncta showing NPY-mCherry in DCVs. *A*, right, cartoon illustration showing only mobile puncta to facilitate interpretation of the kymograph. Note that all green puncta move at slow speed in one direction (left to right in the kymograph), thereby defining anterograde transport. Red puncta move at higher speeds in both directions. *B–E*, comparison of 78 tracked vesicles in anterograde and 67 tracked vesicles in retrograde direction in 3 different mice. MW test showed significant difference in mean and maximal speed as well as in pausing time and unidirectionality factor (*P* values: < 0.0001, 0.0002, 0.0021, < 0.0001) *F*, comparison of mean speeds within axons showing more than 2 vesicles in each direction.

expression did not artificially induce DCV biogenesis and, therefore, our study reports physiologically relevant processes. In addition to axonal fluorescent clusters, we also regularly found larger fluorescent clusters outside the axons. These clusters may reflect autofluorescent cellular debris near the pial surface, stable deposits of secreted DCV cargo or endocytosed fluorescent proteins within scavenger cells such as astrocytes or microglia, or in neurons. Such accumulations of DCV cargo after their release is a well-known phenomenon in coelomocytes of the nematode *C. elegans* (Zahn *et al.* 2004).

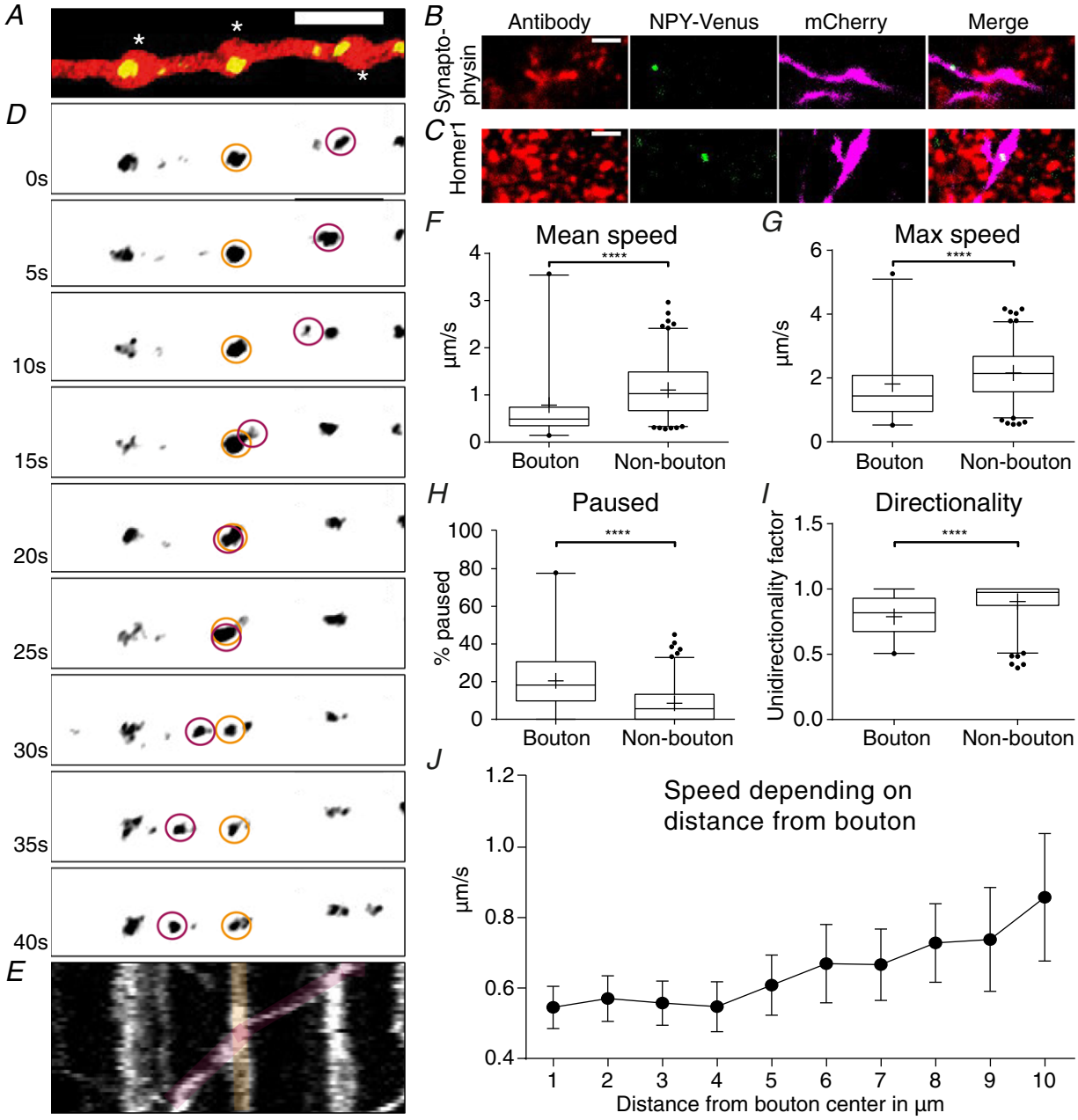

Figure 7. Reduced DCV trafficking speed at *en-passant* boutons
A, single two-photon frame showing a mCherry-labelled axon containing NPY-Venus puncta, white asterisks indicate *en-passant* boutons. *B* and *C*, three colour labelling as indicated next to the panels. Average intensity projections of 5 consecutive confocal image planes. Scale bar, 2 μm. *D*, time-lapse images of NPY-Venus puncta. Stationary DCV (orange circle) and moving/pausing DCV (red circle). Scale bar, 5 μm. *E*, kymograph of time-lapse in *D*. *F–I*, comparison of 245 tracks from axons lacking boutons with 57 tracks from axons having visible boutons. The groups are significantly different in all analysed trafficking characteristics (Mann-Whitney test; *P* values < 0.0001). *J*, mean speeds of tracks in relation to their distance to the bouton.

The DCV velocities and directionality of their transport determined here generally correspond well with previously reported data from *in vitro* experiments and studies in other model systems (Zahn *et al.* 2004; de Wit *et al.* 2006; Barkus *et al.* 2008; Kwinter *et al.* 2009; Bittins *et al.* 2010). The higher peak speed and shorter pausing time observed *in vivo* might be due to different temperatures in cell culture experiments or the fact that axonal microtubule orientation is different in mammals and invertebrates (del Castillo *et al.* 2015). Furthermore, neuronal activity patterns are probably different *in vitro* and *in vivo* and lead to a different amount of arrest, as DCV arrest is induced by activity (de Wit *et al.* 2006). Finally, we observed a wide range of DCV trafficking patterns: Faster vesicles passing slower ones in the same direction, vesicles first travelling alone, then together to finally be separated again, vesicles passing each other in different directions, most vesicles slowing down mid-travel to pause for a short time and others travelling with a constant speed over the whole tracked distance. The frequent changes in movement speed and also directionality may be due to different motor proteins of the kinesin family bound to the same vesicle, possibly in combination with a dynein motor, thereby defining the speed of the vesicles as a product of the individual speeds of the motors involved (Gumy *et al.* 2017). Another reason for the directionality changes might be switching between different motor proteins. These diverse *in vivo* trafficking patterns resemble patterns previously observed *in vitro* (de Wit *et al.* 2006). In conclusion, the general properties of DCV trafficking in the intact mouse brain are in agreement with previous findings in neuronal primary cell culture and invertebrates. This may be attributed to the high conservation of motor proteins that are responsible for DCV transport in all investigated model systems (Zahn *et al.* 2004; Barkus *et al.* 2008).

Coexpression of the microtubule marker MACF18-GFP with the DCV marker NPY-mCherry allowed us to distinguish between anterogradely and retrogradely moving DCVs. The mean speed of all anterogradely travelling DCVs was 2.14 μm/s, approximately 50% faster than vesicles moving retrogradely, at 1.4 μm/s. This is in accordance with findings from cultured hippocampal neurons, but in opposition to findings at *Drosophila* neuromuscular junction, where DCVs move antero- and retrogradely at roughly the same speed (Shakiryanova *et al.* 2006; Barkus *et al.* 2008). Our findings are consistent with speeds reported for motor proteins recruited for axonal anterograde and retrograde movement, with kinesins moving DCVs considerably faster than dynein (Maday *et al.* 2014). The overall higher mean speed reported in Fig. 6 compared with that reported in Fig. 4 might be attributed to the fact that we only analysed axonal stretches containing multiple moving DCVs, potentially interfering with trafficking speed. Furthermore, overexpression of MACF18-GFP might enhance microtubule growth rate or stabilize microtubules. This could lead to elongation of microtubule tracks and thus less pausing and higher mean speeds. In conclusion, the anterograde trafficking speed of DCVs is approximately 50% faster than retrograde transport *in vivo*.

MACF18-GFP allowed us to monitor axonal microtubule dynamics in the cerebral cortex *in vivo*. We found a unidirectional polarity of axonal movement of microtubules *in vivo* with a comet run length of around 10 μm. In comparison to developing neurons, the number of moving comets/unit of axon length is relatively small (Conde & Cáceres, 2009). The mean speed of comet growth was 0.12 μm/s, in agreement with findings of other *in vivo* studies in spinal cord axons of 0.147 μm/s (Kleele *et al.* 2014) and 0.09 μm/s in dendrites of cortical neurons (Yau *et al.* 2016).

The newly discovered reduction in transport speed and longer pausing times at axonal *en-passant* boutons may be a mechanism to increase the availability of DCVs at presynaptic sites (Wong *et al.* 2012), consistent with the notion that these sites accumulate the protein complexes that drive exocytosis and are the main locations of DCV capture and release (Torrealba & Carrasco, 2004). The mechanism that reduces DCV speed remains unclear. Several mutually non-exclusive possibilities are plausible. (1) Axonal *en-passant* boutons are small compartments packed with proteins, mitochondria and synaptic vesicles. Molecular (or organelle-) crowding could contribute to slowing of DCV transport through these structures, as indicated by diffusion models in boutons (Wragg *et al.* 2015). (2) DCVs are mainly transported via microtubule-mediated transport mechanisms (Barkus *et al.* 2008). The slowing could be caused by shorter microtubule tracks in and around boutons, causing more frequent switches between tracks, in turn leading to an effective slowing and more frequent directional changes. (3) Microtubule-mediated transport is regulated through post-translational modifications of tubulins (Schlager *et al.* 2009), or motor proteins (Akhmanova & Hammer, 2010; Hirokawa *et al.* 2010). Synapses may accumulate kinases and other modifying enzymes to specifically affect trafficking speed at synapses. (4) DCVs are not only transported via microtubule-dependent motors, but also via actin-dependent myosin motors (Bittins *et al.* 2010). The presynaptic actin-myosin network may play a role in tethering DCVs to the membrane and in DCV release (Papadopulos *et al.* 2015). The highly local actin-myosin motors may also contribute to the slowing of DCV transport at presynaptic boutons. (5) Finally, fast axonal transport of DCVs is known to be inhibited by activity in a Ca^{2+}-dependent manner (de Wit *et al.* 2006). Because Ca^{2+}-channels are known to accumulate in presynaptic specializations, endogenous activity in the axons will preferentially increase intracellular free Ca^{2+} in boutons and slow down DCV trafficking in this area. However,

the slowing effect was also observed in anaesthetized mice, presumed to have a lower neuronal activity. Taken together, a number of possible mechanisms may explain the slowing of DCVs in axonal boutons to increase their availability at presynaptic sites.

References

Akhmanova A & Hammer JA (2010). Linking molecular motors to membrane cargo. *Curr Opin Cell Biol* **22**, 479–487.

Barkus R V, Klyachko O, Horiuchi D, Dickson BJ & Saxton WM (2008). Identification of an axonal kinesin-3 motor for fast anterograde vesicle transport that facilitates retrograde transport of neuropeptides. *Mol Biol Cell* **19**, 274–283.

Berbel P & Innocenti GM (1988). The development of the corpus callosum in cats: a light- and electron-microscopic study. *J Comp Neurol* **276**, 132–156.

Bittins CM, Eichler TW, Hammer JA & Gerdes H-H (2010). Dominant-negative myosin Va impairs retrograde but not anterograde axonal transport of large dense core vesicles. *Cell Mol Neurobiol* **30**, 369–379.

Cohen S & Greenberg ME (2008). Communication between the synapse and the nucleus in neuronal development, plasticity, and disease. *Annu Rev Cell Dev Biol* **24**, 183–209.

Conde C & Cáceres A (2009). Microtubule assembly, organization and dynamics in axons and dendrites. *Nat Rev Neurosci* **10**, 319–332.

del Castillo U, Winding M, Lu W & Gelfand VI (2015). Interplay between kinesin-1 and cortical dynein during axonal outgrowth and microtubule organization in Drosophila neurons. *Elife* **4**, e10140.

Denk W, Delaney KR, Gelperin A, Kleinfeld D, Strowbridge BW, Tank DW & Yuste R (1994). Anatomical and functional imaging of neurons using 2-photon laser scanning microscopy. *J Neurosci Methods* **54**, 151–162.

de Wit J, Toonen RF, Verhaagen J & Verhage M (2006). Vesicular trafficking of semaphorin 3a is activity-dependent and differs between axons and dendrites. *Traffic* **7**, 1060–1077.

de Wit J, Toonen RF & Verhage M (2009). Matrix-dependent local retention of secretory vesicle cargo in cortical neurons. *J Neurosci* **29**, 23–37.

Farina M, van de Bospoort R, He E, Persoon CM, van Weering JRT, Broeke JH, Verhage M & Toonen RF (2015). CAPS-1 promotes fusion competence of stationary dense-core vesicles in presynaptic terminals of mammalian neurons. *Elife* **4**, e05438.

Gumy LF, Katrukha EA, Grigoriev I, Jaarsma D, Kapitein LC, Akhmanova A & Hoogenraad CC (2017). MAP2 defines a pre-axonal filtering zone to regulate KIF1- *versus* KIF5-dependent cargo transport in sensory neurons. *Neuron* **94**, 347–362.e7.

Hartmann M, Heumann R & Lessmann V (2001). Synaptic secretion of BDNF after high-frequency stimulation of glutamatergic synapses. *EMBO J* **20**, 5887–5897.

Hirokawa N, Niwa S & Tanaka Y (2010). Molecular motors in neurons: transport mechanisms and roles in brain function, development, and disease. *Neuron* **68**, 610–638.

Holtmaat A, Bonhoeffer T, Chow DK, Chuckowree J, De Paola V, Hofer SB, Hübener M, Keck T, Knott G, Lee W-CA, Mostany R, Mrsic-Flogel TD, Nedivi E, Portera-Cailliau C, Svoboda K, Trachtenberg JT & Wilbrecht L (2009). Long-term, high-resolution imaging in the mouse neocortex through a chronic cranial window. *Nat Protoc* **4**, 1128–1144.

Huang EJ & Reichardt LF (2001). Neurotrophins: roles in neuronal development and function. *Annu Rev Neurosci* **24**, 677–736.

Kim T, Gondré-Lewis MC, Arnaoutova I & Loh YP (2006). Dense-core secretory granule biogenesis. *Physiology (Bethesda)* **21**, 124–133.

Kleele T, Marinković P, Williams PR, Stern S, Weigand EE, Engerer P, Naumann R, Hartmann J, Karl RM, Bradke F, Bishop D, Herms J, Konnerth A, Kerschensteiner M, Godinho L & Misgeld T (2014). An assay to image neuronal microtubule dynamics in mice. *Nat Commun* **5**, 4827.

Komarova Y, Lansbergen G, Galjart N, Grosveld F, Borisy GG & Akhmanova A (2005). EB1 and EB3 control CLIP dissociation from the ends of growing microtubules. *Mol Biol Cell* **16**, 5334–5345.

Kwinter DM, Lo K, Mafi P & Silverman MA (2009). Dynactin regulates bidirectional transport of dense-core vesicles in the axon and dendrites of cultured hippocampal neurons. *Neuroscience* **162**, 1001–1010.

Lo KY, Kuzmin A, Unger SM, Petersen JD & Silverman MA (2011). KIF1A is the primary anterograde motor protein required for the axonal transport of dense-core vesicles in cultured hippocampal neurons. *Neurosci Lett* **491**, 168–173.

Maday S, Twelvetrees AE, Moughamian AJ & Holzbaur ELF (2014). Axonal transport: cargo-specific mechanisms of motility and regulation. *Neuron* **84**, 292–309.

Meyer-Lindenberg A, Domes G, Kirsch P & Heinrichs M (2011). Oxytocin and vasopressin in the human brain: social neuropeptides for translational medicine. *Nat Rev Neurosci* **12**, 524–538.

Papadopulos A, Gomez GA, Martin S, Jackson J, Gormal RS, Keating DJ, Yap AS & Meunier FA (2015). Activity-driven relaxation of the cortical actomyosin II network synchronizes Munc18-1-dependent neurosecretory vesicle docking. *Nat Commun* **6**, 6297.

Preibisch S, Saalfeld S, Schindelin J & Tomancak P (2010). Software for bead-based registration of selective plane illumination microscopy data. *Nat Methods* **7**, 418–419.

Reichmann F & Holzer P (2015). Neuropeptide Y: A stressful review. *Neuropeptides* **55**, 99–109.

Rose JB, Crews L, Rockenstein E, Adame A, Mante M, Hersh LB, Gage FH, Spencer B, Potkar R, Marr RA & Masliah E (2009). Neuropeptide Y fragments derived from neprilysin processing are neuroprotective in a transgenic model of Alzheimer's disease. *J Neurosci* **29**, 1115–1125.

Samson AL & Medcalf RL (2006). Tissue-type plasminogen activator: a multifaceted modulator of neurotransmission and synaptic plasticity. *Neuron* **50**, 673–678.

Schlager MA & Hoogenraad CC (2009). Basic mechanisms for recognition and transport of synaptic cargos. *Mol Brain* **2**, 25.

Schwenger DB & Kuner T (2010). Acute genetic perturbation of exocyst function in the rat calyx of Held impedes structural maturation, but spares synaptic transmission. *Eur J Neurosci* **32**, 974–984.

Seitz A & Surrey T (2006). Processive movement of single kinesins on crowded microtubules visualized using quantum dots. *EMBO J* **25**, 267–277.
Shakiryanova D, Tully A & Levitan ES (2006). Activity-dependent synaptic capture of transiting peptidergic vesicles. *Nat Neurosci* **9**, 896–900.
Taraska JW, Perrais D, Ohara-Imaizumi M, Nagamatsu S & Almers W (2003). Secretory granules are recaptured largely intact after stimulated exocytosis in cultured endocrine cells. *Proc Natl Acad Sci U S A* **100**, 2070–2075.
Tinevez J-Y, Perry N, Schindelin J, Hoopes GM, Reynolds GD, Laplantine E, Bednarek SY, Shorte SL & Eliceiri KW (2016). TrackMate: An open and extensible platform for single-particle tracking. *Methods* **115**, 80–90.
Torrealba F & Carrasco MA (2004). A review on electron microscopy and neurotransmitter systems. *Brain Res Brain Res Rev* **47**, 5–17.
Wimmer V, Nevian T & Kuner T (2004). Targeted in vivo expression of proteins in the calyx of Held. *Pflugers Arch* **449**, 319–333.
van de Bospoort R, Farina M, Schmitz SK, de Jong A, de Wit H, Verhage M & Toonen RF (2012). Munc13 controls the location and efficiency of dense-core vesicle release in neurons. *J Cell Biol* **199**, 883–891.
van den Pol AN (2012). Neuropeptide transmission in brain circuits. *Neuron* **76**, 98–115.
Wong MY, Zhou C, Shakiryanova D, Lloyd TE, Deitcher DL & Levitan ES (2012). Neuropeptide delivery to synapses by long-range vesicle circulation and sporadic capture. *Cell* **148**, 1029–1038.
Wragg RT, Gouzer G, Bai J, Arianna G, Ryan TA & Dittman JS (2015). Synaptic activity regulates the abundance and binding of complexin. *Biophys J* **108**, 1318–1329.
Yau KW, Schätzle P, Tortosa E, Pagès S, Holtmaat A, Kapitein LC & Hoogenraad CC (2016). Dendrites *in vitro* and in vivo contain microtubules of opposite polarity and axon formation correlates with uniform plus-end-out microtubule orientation. *J Neurosci* **36**, 1071–1085.
Zahn TR, Angleson JK, MacMorris MA, Domke E, Hutton JF, Schwartz C & Hutton JC (2004). Dense core vesicle dynamics in *Caenorhabditis elegans* neurons and the role of kinesin UNC-104. *Traffic* **5**, 544–559.

Additional information

Competing interests

The authors declare that they have no competing financial interests.

Author contributions

T.K. and M.V. designed the experiments, J.K. and J.P.N. carried out all experiments and analyses. All authors contributed to data interpretation. J.K. drafted the initial manuscript which was completed by T.K. and all other authors. All authors approved the final version submitted for publication and agree to be accountable for all aspects of the work in ensuring that questions related to the accuracy and integrity of any part of the work are appropriately investigated and resolved. All persons designated as authors qualify for authorship, and all those who qualify are listed.

Funding

T.K. was supported by the German Science Foundation CellNetworks Cluster of Excellence (EXC81). J.K. and J.P.N. were supported by internal resources of the Department of Functional Neuroanatomy. We gratefully acknowledge the data storage service SDS@hd supported by the Ministry of Science, Research and the Arts Baden-Württemberg (MWK) and the German Research Foundation (DFG) through grant INST 35/1314-1 FUGG.

Acknowledgements

We thank Michaela Kaiser and Claudia Kocksch for excellent technical assistance, Ruud Toonen, Jurjen Broeke, Rhode van Westen and Claudia Persoon for discussions during the ongoing project, as well as Ralph Nawrotzki for the kind gifts of LC-3, Lamp-2, Rab5 antibodies.

Supporting information

Additional supporting information may be found online in the Supporting Information section at the end of the article.

Supporting Movie S1. DCVs trafficking through thalamocortical axons imaged in an anaesthetized mouse in vivo. Original frame rate: 1 Hz, sped up to 15 Hz. Movie relates to Fig. 3.
Supporting Movie S2. DCVs trafficking through thalamocortical axons imaged in an awake mouse in vivo. Original frame rate: 1 Hz, sped up to 15 Hz. Movie relates to Fig. 4.
Supporting Movie S3. Microtubule +-end extension imaged in an anaesthetized mouse in vivo. Original frame rate: 1 Hz, sped up to 10 Hz. Movie relates to Fig. 5.
Supporting Movie S4. Slowing of DCVs at presynaptic boutons imaged in an anaesthetized mouse in vivo. Original frame rate: 1 Hz, sped up to 15 Hz. Movie relates to Fig. 7.